Height of a liquid drop on a wetting stripe

Alexandr Malijevský

Department of Physical Chemistry, University of Chemical Technology Prague, Praha 6, 166 28,
Czech Republic; The Czech Academy of Sciences, Institute of Chemical Process Fundamentals,
Department of Molecular Modelling, 165 02 Prague, Czech Republic

Adsorption of liquid on a planar wall decorated by a hydrophilic stripe of width L is considered. Under the condition, that the wall is only partially wet (or dry) while the stripe tends to be wet completely, a liquid drop is formed above the stripe. The maximum height $\ell_m(\delta\mu)$ of the drop depends on the stripe width L and the chemical potential departure from saturation $\delta\mu$ where it adopts the value $\ell_0 = \ell_m(0)$. Assuming a long-range potential of van der Waals type exerted by the stripe, the interfacial Hamiltonian model is used to show that ℓ_0 is approached linearly with $\delta\mu$ with a slope which scales as L^2 over the region satisfying $L \lesssim \xi_\parallel$, where $\xi_\parallel$ is the parallel correlation function pertinent to the stripe. This suggests that near the saturation there exists a universal curve $\ell_m(\delta\mu)$ to which the adsorption isotherms corresponding to different values of L all collapse when appropriately rescaled. Although the series expansion based on the interfacial Hamiltonian model can be formed by considering higher order terms, a more appropriate approximation in the form of a rational function based on scaling arguments is proposed. The approximation is based on exact asymptotic results, namely that $\ell_m \sim \delta\mu^{-1/3}$ for $L \to \infty$ and that ℓ_m obeys the correct $\delta\mu \to 0$ behaviour in line with the results of the interfacial Hamiltonian model. All the predictions are verified by the comparison with a microscopic density functional theory (DFT) and, in particular, the rational function approximation—even in its simplest form—is shown to be in a very reasonable agreement with DFT for a broad range of both $\delta\mu$ and L.

I. INTRODUCTION

It is well known that under certain conditions near the bulk liquid-gas coexistence, a macroscopic amount of liquid may intrude at the wall-gas interface, making the wall completely wet [1–7]. Similarly, in magnetic systems a ferromagnet may be induced near a surface whose coupling with the spins is sufficiently strong, while the bulk remains disordered. For fluid systems, the nature of adsorption depends on the thermodynamic path and also on the microscopic forces determining both fluid-fluid and wall-fluid interactions between the atoms. In particular, at a fixed (subcritical) temperature $T > T_w$, where T_w is the wetting temperature at which Young's contact angle, made by the interface of the fluid coexisting phases and the wall, becomes zero, the mean height ℓ_π of the adsorbed liquid film grows continuously and (in the absence of gravity) diverges as the bulk liquid-gas coexistence is approached from below. This critical phenomenon is called complete wetting and is also characterized by a divergence of the parallel correlation

length $\xi_\parallel$ along the liquid-gas interface. The departure of the given thermodynamic state from the bulk liquid-gas coexistence can be quantified by the chemical potential difference $\delta\mu = \mu_{\mathrm{sat}}(T) - \mu$ from its saturation value $\mu_{\mathrm{sat}}(T)$. In the presence of long-range microscopic forces, which asymptotically decay according to the power-law, the film thickness and the parallel correlation length diverge as [8]

$$\ell_\pi(\delta\mu) \sim \delta\mu^{-\beta}, \tag{1}$$

and

$$\xi_\parallel(\delta\mu) \sim \delta\mu^{-\nu_\parallel}, \tag{2}$$

as $\delta\mu \to 0$, where the value of the critical exponents reflect the asymptotic behaviour of the microscopic forces. In particular, for non-retarded dispersion forces, which can be modelled by the familiar Lennard-Jones potential, $\beta = 1/3$ and $\nu_\parallel = 2/3$ [8].

If the adsorbing wall is heterogenous, such that its surface is modified chemically or geometrically, the wetting phenomena become considerably more intricate in comparison with a homogenous and perfectly flat wall considered above. The process of complete wetting may then be accompanied by a plenty of other interfacial phenomena such as filling [9–22], unbending [23–25], depinning [26–28], bridging [29–31] and other morphological transitions [32–42], whose interplay may give rise to very complex phase behaviour of the adsorbed fluid. In this work, let us consider a substrate (wall) which is flat but decorated by a macroscopically long stripe of width L which is of a material with a greater affinity to the liquid phase than the rest of the wall, such that its wetting temperature T_w^{stripe} is lower than the wetting temperature of the wall T_w^{wall}.
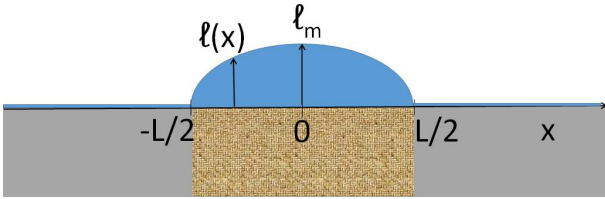

FIG. 1: A schematic two-dimensional projection of a liquid drop on a wetting stripe of width L. The remaining part of the wall is of a different material and is only in a partially wetting state.

Therefore, considering a temperature T which is in between the two wetting temperatures, $T_w^{\text{stripe}} < T < T_w^{\text{wall}}$, the stripe will tend to become completely wet, in contrast to the surrounding wall which is only in a partially wetting state. This means that sufficiently close to the bulk phase coexistence, a liquid cylindrical drop forms above the stripe whose local height $\ell(x)$ has a maximum ℓ_m in the middle of the stripe and is pinned to the wall at the stripe edges (see Fig. 1). The properties of liquid drops on heterogeneous walls have been studied previously [43–48] at the bulk fluid coexistence in two [45–47] and three [43, 44, 48] dimensions. Systems involving only short-range forces have been shown to exhibit conformal invariance which allows to predict the explicit form of the droplet height for a number of different domain shapes [43]; this is no more the case of systems with the long-range forces which, however, still exhibit some scale invariance for the shape of the drop and its height which scales with the width of the stripe as $\ell_m \propto \sqrt{L}$ [48].

The purpose of this work is to extend these studies by considering the growth of the drop as the saturation is approached from below. This means, that we study the process of restricted, finite-size complete wetting and wish to know how the growth of the drop depends on two parameters: $\delta\mu$ and L. To this end, we first briefly recapitulate the mean-field analysis based on the interfacial Hamiltonian model leading to the simple formula for the height of the drop at saturation, $\delta\mu = 0$. Next, the analysis is extended to the case of $\delta\mu > 0$ which, however, does not yield a solution in a closed form but can be expressed as a series in a dimensionless parameter proportional to $\delta\mu$. Although this allows to obtain the asymptotic properties of the droplet growth upon approaching the saturation, the series expansion analysis is restricted only to a vicinity of the saturation which thins with increasing the stripe width. Therefore, an alternative approach invoking finite-size scaling arguments will be followed by taking advantage of the known droplet behaviour in the limits of $L \to \infty$ and $\delta\mu \to 0$. This leads to a representation of the droplet height in the form of a rational function of a single scaling parameter involving both $\delta\mu$ and L with coefficients determined by requiring a consistency with the series expansion for small $\delta\mu$ obtained previously from the interfacial Hamiltonian. In this way, a very simple approximation for the droplet growth is found which, together with the series expansions up to the third order, will be compared with the results obtained from a classical density functional theory for a wide range of stripe widths.

II.   ANALYTICAL CALCULATIONS

On a mesoscopic level, a theoretical study of interfacial phenomena is based on an analysis of effective Hamiltonian models $H[\ell]$ [8], which describe the system state in terms of a shape $\ell(x)$ of the liquid-gas interface. This approach has been used with a great success in the theory of wetting phenomena on a homogenous planar wall but has also been applied in various modified forms for other model substrates. In this work, we will consider a simple interfacial model, which is defined by the following Hamiltonian per unit length

$$H[\ell] = \int_{-L/2}^{L/2} \mathrm{d}x \left[\frac{\gamma}{2} \left(\frac{\mathrm{d}\ell(x)}{\mathrm{d}x} \right)^2 + W(\ell(x)) \right]. \qquad (3)$$

In a close analogy with the analytical mechanics, the effective Hamiltonian consists of two terms, where the first, "kinetic" contribution proportional to the liquid-gas surface tension γ is a free energy penalty for bending the interface. Here, we suppose that the interface follows the symmetry of the wall and thus varies in only one dimension which is the Cartesian axis x and is translation invariant along the stripe corresponding to axis y. The second term of the functional is the so called binding potential $W(\ell)$ which describes the free-energy cost for the presence of the liquid drop including the effect of microscopic forces.

At mean-field level, the equilibrium interface profile is found by simply minimizing (3), leading to the Euler-Lagrange equation

$$\gamma \frac{\mathrm{d}^2\ell}{\mathrm{d}x^2} = W'(\ell), \qquad (4)$$

which is a subject of the boundary conditions $\ell(L/2) = \ell(-L/2) = 0$ and $\frac{\mathrm{d}\ell(0)}{\mathrm{d}x} = 0$. Here, an irrelevant but fixed microscopic height of the interface at the stripe edges was set to zero. After integrating (4) once and applying the boundary condition, one obtains

$$\frac{\gamma}{2} \left(\frac{\mathrm{d}\ell}{\mathrm{d}x} \right)^2 = W(\ell) - W(\ell_m) \qquad (5)$$

where $\ell_m = \ell(0)$ is the maximum height of the drop. Further integration leads to the expression for the interface profile in the form of

$$\int_{\ell(x)}^{\ell_m} \frac{\mathrm{d}\ell'}{\sqrt{W(\ell') - W(\ell_m)}} = \sqrt{\frac{2}{\gamma}} |x|, \qquad (6)$$

which for $x = L/2$ yields an equation determining ℓ_m:

$$\int_0^{\ell_m} \frac{\mathrm{d}\ell}{\sqrt{W(\ell) - W(\ell_m)}} = \frac{L}{\sqrt{2\gamma}}. \qquad (7)$$

Eqs. (6) and (7) are the general expressions for $\ell(x)$ and ℓ_m, respectively, which follow exactly from the Euler-Lagrange equation (4). We now consider the specific but experimentally most relevant case, when the stripe interacts with the fluid via the long-range dispersion forces. For a sufficiently large L this implies the following form of the binding potential

$$W(\ell) = \delta\mu\Delta\rho\ell + \frac{A}{\ell^2} + \dots \qquad (8)$$

where the Hamaker constant $A > 0$, since $T > T_w^{\text{stripe}}$ and where the ellipses denote higher order terms in $1/\ell$. Here, the first term linear in ℓ is the volume free-energy cost due to the occurrence of the metastable liquid, where $\Delta\rho = \rho_l(T) - \rho_v(T)$ is the density difference between the liquid and gas particle densities of the bulk phases coexisting at the given temperature; the second term which decays as ℓ^{-2} reflects the presence of the dispersion forces. When applied to a planar wall (corresponding to $L \to \infty$), in which case the l.h.s. of (4) is zero, the equilibrium film thickness ℓ_π is given by a minimization of the binding potential, which implies

$$\ell_\pi = \left(\frac{2A}{\delta\mu\Delta\rho}\right)^{\frac{1}{3}}, \qquad (9)$$

as $\delta\mu \to 0$, in line with the general result of Eq. (1). One can also check that the value of the critical exponent for the parallel correlation length according to the binding potential (8) has the expected value $\nu_\parallel = 2/3$, since $\xi_\parallel \propto \sqrt{1/W''}$ as follows from the Ornstein-Zernike theory [6].

At saturation, i.e. for $\delta\mu = 0$, the inverse quadratic form of the binding potential allows for a simple explicit solution for the droplet height. In this case, a substitution of (8) into (6) leads to

$$\ell(x) = \sqrt{\ell_0^2 - \frac{2A}{\gamma}\frac{x^2}{\ell_0^2}} \qquad (10)$$

where the abbreviation for the the droplet maximum height at saturation $\ell_0 \equiv \ell_m(\delta\mu = 0)$ has been introduced, which itself satisfies

$$\ell_0^2 = \sqrt{\frac{A}{2\gamma}}L, \qquad (11)$$

thus $\ell_0 \propto \sqrt{L}$.

We now wish to extend these results below saturation, i.e. for $\delta\mu > 0$. Substituting (8) to (7) leads after some rearranging to

$$\frac{L}{\ell_m^2}\sqrt{\frac{A}{2\gamma}} = \int_0^1 \frac{u\,\mathrm{d}u}{\sqrt{1 - u^2 - 2cu^2(1-u)}} \qquad (12)$$

where $c \equiv \delta\mu\Delta\rho\ell_m^3/2A$, and using Eq. (11) one obtains

$$\frac{\ell_0^2}{\ell_m^2} = \int_0^1 \frac{u\,\mathrm{d}u}{\sqrt{1 - u^2 - 2cu^2(1-u)}} \qquad (13)$$

Note that with the help of Eq. (9) the dimensionless parameter c can also be expressed as $c = (\ell_m/\ell_\pi)^3$, hence $0 \le c < 1$, such that $c \to 0$ as $\delta\mu \to 0$ for L fixed. Since we could not find the exact solution of Eq. (13) by evaluating the integral, we proceed in a perturbative manner and expand the r.h.s. of Eq. (13) around $c = 0$ for which the solution is known and given by Eq. (11). Thus, we can write

$$\frac{\ell_0^2}{\ell_m^2} = 1 + a_1 c + a_2 c^2 + a_3 c^3 + \dots, \qquad (14)$$

where the first coefficients are

$$a_1 = \frac{3}{4}\pi - 2, \qquad (15)$$

$$a_2 = 12 - \frac{15}{4}\pi, \qquad (16)$$

$$a_3 = \frac{735}{32}\pi - 72. \qquad (17)$$

To lowest order (linear in c), Eq. (14) can be recast into

$$a_1\varepsilon x^5 + x^2 = 1 \qquad (18)$$

with $x \equiv \ell_m/\ell_0$ and $\varepsilon \equiv \ell_0^3/\ell_\pi^3$. We seek the solution of Eq. (18) in the form of $x(\varepsilon) = 1 + x_1\varepsilon + \dots$, which gives

$$x = 1 - \frac{a_1}{2}\varepsilon + \cdots, \qquad (19)$$

hence we obtain that

$$\ell_m \approx \ell_0\left[1 - \left(\frac{3}{8}\pi - 1\right)\frac{\ell_0^3}{\ell_\pi^3}\right]. \qquad (20)$$

The linear (in ε and thus in $\delta\mu$) form of Eq. (20) assumes that the higher order terms of the expansion can be neglected, which requires $\delta\mu$ small enough, such that $\ell_0 < \ell_\pi$. Hence the condition, under which the linear approximation (20) may be deemed reliable, can be expressed with the help of Eqs. (9) and (11) as

$$L < \frac{A^{1/6}\sqrt{2\gamma}}{(\Delta\rho\delta\mu)^{\frac{2}{3}}} \propto \xi_\parallel, \qquad (21)$$

where the right hand side which diverges as $\delta\mu^{-2/3}$ for small $\delta\mu$ has been associated with the parallel correlation length.

The lowest order approximation given by Eq. (20) is sufficient for a description of the asymptotic behaviour of the droplet height approaching its saturation value ℓ_0. Thus, near the saturation, such that the condition (21) is satisfied, the dependence $\ell_m(\delta\mu)$ is linear in $\delta\mu$ with a slope which scales quadratically with L. Furthermore, Eq. (20) suggests a universal behaviour of the droplet growth in the rescaled variables $\widetilde{\ell_m} = \ell_m/\sqrt{L}$ and $\widetilde{\delta\mu} = \delta\mu L^{3/2}$. We will come back to this in section 4 where these predictions will be tested against a microscopic DFT.

One can expect that by accounting for higher order terms in expansion (14) an improvement over the linear approximation (20) can be achieved. For instance, up to the third order, Eq. (18) will be modified as follows

$$1 = x^2 + a_1 x^5\varepsilon + a_2 x^8\varepsilon^2 + a_3 x^{11}\varepsilon^3, \qquad (22)$$

whose solution can be sought in the form of $x(\varepsilon) = 1 + x_1\varepsilon + x_2\varepsilon^2 + x_3\varepsilon^3$, where the coefficients of the expansion are $x_1 = -a_1/2$ (reproducing Eq. (20)), $x_2 = 9/8a_1^2 - a_2/2$, and $x_3 = 3a_1a_2 - 7/2a_1^3 - a_3/2$. However,

although the inclusion of the higher order terms in the series expansion is expected to provide a better approximation compared to Eq. (20), the condition (21) must still be obeyed meaning that its performance worsens with L.

To obtain a more general approximation, one should seek an alternative representation of $\ell(\delta\mu)$. In fact, since a planar wall is the natural reference system for our model, the approximate solution should be increasingly more reliable as the stripe width extends, becoming exact in the limit of $L \to \infty$, for which the planar solution $\ell_\pi(\delta\mu)$ should be reproduced. Note that this contrasts with the series expansion representation, whose range of applicability shrinks with increasing L. Therefore, let us assume the solution in the form of

$$\ell_m = \ell_\pi \Phi \left(\frac{\ell_0}{\ell_\pi} \right) , \qquad (23)$$

where the scaling function Φ, which is a finite-size correction to complete wetting, satisfies the conditions: $\Phi(t) = 1$, as $t \to \infty$ and $\Phi(t) = t$ as $t \to 0$. Alternatively, the scaling function could be written as $\tilde{\Phi}(L/\xi_\parallel)$, satisfying $\tilde{\Phi}(t) \propto t^{1/2}$ as $t \to 0$ but Eq. (23) is more appropriate for the further analysis and suggests the following form of ℓ_m:

$$\ell_m = \ell_\pi \frac{\sum_{i=1}^n a_i t^i}{1 + \sum_{i=1}^n b_i t^i} , \qquad (24)$$

where $t = \ell_0/\ell_\pi$ and where the behaviour of the scaling function implies that $a_1 = 1$ and $a_n = b_n$.

Thus, requirements put on the correct behaviour of $\ell(\delta\mu)$ in the limit of $L \to \infty$ and for $\delta\mu = 0$ imply that its form should follow the rational function expansion (24), which in the lowest order reduces to an additive rule for the reciprocals of all the present film thicknesses: $\ell_m^{-1} = \ell_\pi^{-1} + \ell_0^{-1}$. However, such a remarkably simple expression does not comply with the correct linear behaviour of $\ell_m(\delta\mu)$ near the saturation, which is the exact result of the interfacial Hamiltonian model in the limit of $\delta\mu \to 0$. Therefore, the correct asymptotic behavior (20) of the liquid growth is used as an additional constraint imposed on the rational function approximation, which implies that its simplest form is of the third order:

$$\ell_m = \ell_\pi \frac{t + at^2 + bt^3}{1 + ct + dt^2 + bt^3} . \qquad (25)$$

The condition (20) then determines two of the coefficients, namely that $b = d = a_1$. The other two coefficients a and c are undetermined, except that they must be equal. Since we do not impose any further conditions on the behaviour of $\ell_m(\delta\mu)$, they might be set to zero, which, moreover, guarantees the absence of the term proportional to $(\delta\mu)^{4/3}$ in the Taylor expansion of (25). Finally, we get

$$\frac{\ell_m}{\ell_0} = \frac{1 + a_1 t^2}{1 + a_1 t^2 + a_1 t^3} . \qquad (26)$$

This is the rational function approximation for the droplet height which we propose and whose accuracy will be tested in section IV by a comparison with DFT.

III. DENSITY FUNCTIONAL THEORY

Classical density functional theory [49] is a statistical mechanical tool to determine thermodynamic properties and correlation functions of inhomogeneous fluids. It is based on the result that the grand potential of a molecular system is a functional of one-body particle density $\rho(\mathbf{r})$ and its minimum with respect to $\rho(\mathbf{r})$ determines the equilibrium density profile and the thermodynamic free energy. The grand potential is related to the intrinsic Helmholtz free energy $\mathcal{F}$ via the functional Legendre transform

$$\Omega[\rho] = \mathcal{F}[\rho] + \int d\mathbf{r}\rho(\mathbf{r})[V(\mathbf{r}) - \mu] , \qquad (27)$$

where μ is the chemical potential and $V(\mathbf{r})$ is an external field experienced by each particle of the system.

Except for a few specific fluid models, the intrinsic free energy functional is not known exactly and must be thus approximated. The scheme of the approximation depends on the model fluid; in particular, for simple fluids of the Lennard-Jones type as considered in this work, it is natural to split the intrinsic free energy into several contributions in a perturbative manner [50]:

$$\mathcal{F}[\rho] = \mathcal{F}_{id}[\rho] + \mathcal{F}_{hs}[\rho] + \mathcal{F}_{att}[\rho] . \qquad (28)$$

Here, $\mathcal{F}_{id}$ is the ideal gas part due to purely entropic effects which is known exactly

$$\beta\mathcal{F}_{id}[\rho] = \int d\mathbf{r}\rho(\mathbf{r}) \left[\ln(\rho(\mathbf{r})\Lambda^3) - 1 \right] , \qquad (29)$$

where Λ is the thermal de Broglie wavelength and $\beta = 1/k_B T$ is the inverse temperature.

The remaining parts of the expansion (28) describe the contribution to the free energy due to the fluid-fluid interaction. Here the fluid pair interaction is described in the spirit of the Barker-Henderson perturbation theory [51], such that it is split as follows

$$u(r) = u_{HS}(r) + u_{att}(r) , \qquad (30)$$

where u_{HS} is the (reference) hard-sphere potential and u_{att} is the attractive tail:

$$u_{att}(r) = \begin{cases} 0 ; & r < \sigma , \\ -4\varepsilon \left(\frac{\sigma}{r} \right)^6 ; & \sigma < r < r_c , \\ 0 ; & r > r_c . \end{cases} \qquad (31)$$

which is truncated at $r_c = 2.5\,\sigma$ and where the parameter σ is identified with the hard-sphere diameter.

The second term of the free-energy expansion (28), $\mathcal{F}_{hs}$, corresponds to the repulsive, hard-sphere part of the

interatomic interaction and is approximated using Rosenfeld's fundamental measure theory (FMT) [52] according to which

$$\mathcal{F}_{\text{hs}}[\rho] = k_B T \int d\mathbf{r}\, \Phi(\{n_\alpha(\mathbf{r})\})\,. \qquad (32)$$

Within FMT, the free energy density Φ depends on the set of weighted densities $\{n_\alpha\}$ which, within the original Rosenfeld approach, consist of four scalar and two vector functions, which are given by convolutions of the density profile and the corresponding weight function:

$$n_\alpha(\mathbf{r}) = \int d\mathbf{r}' \rho(\mathbf{r}') w_\alpha(\mathbf{r} - \mathbf{r}')\ \ \alpha = \{0, 1, 2, 3, v1, v2\}\,, \qquad (33)$$

where $w_3(\mathbf{r}) = \Theta(R - |\mathbf{r}|)$, $w_2(\mathbf{r}) = \delta(R - |\mathbf{r}|)$, $w_1(\mathbf{r}) = w_2(\mathbf{r})/4\pi R$, $w_0(\mathbf{r}) = w_2(\mathbf{r})/4\pi R^2$, $w_{v2}(\mathbf{r}) = \mathbf{r}/R\delta(R - |\mathbf{r}|)$, and $w_{v1}(\mathbf{r}) = w_{v2}(\mathbf{r})/4\pi R$. Here, Θ is the Heaviside function, δ is Dirac's delta function and $R = \sigma/2$.

Finally, the attractive free-energy contribution is treated on a mean-field level:

$$\mathcal{F}_{\text{att}}[\rho] = \frac{1}{2} \int d\mathbf{r}_1 \rho(\mathbf{r}_1) \int d\mathbf{r}_2 \rho(\mathbf{r}_2) u_{\text{att}}(|\mathbf{r}_1 - \mathbf{r}_2|)\,. \quad (34)$$

The external potential $V = V(x, z)$ can be split into the part induced by the wetting stripe which is formed by Lennard-Jones atoms interacting with the fluid atoms via the potential

$$\phi_{\text{stripe}}(r) = 4\varepsilon_w \left[\left(\frac{\sigma}{r} \right)^{12} - \left(\frac{\sigma}{r} \right)^6 \right]\,, \qquad (35)$$

with the strength parameter ε_w.

The remaining part of the wall is assumed to be completely dry, such that the wall atoms interact with the fluid atoms via the repulsive bit of the Lennard-Jones potential:

$$\phi_{\text{wall}}(r) = 4\varepsilon_w \left(\frac{\sigma}{r} \right)^{12}\,. \qquad (36)$$

The entire external potential is obtained by integrating the wall-fluid pair potential over the whole domain of the wall which is assumed to be formed by wall atoms that are distributed uniformly with a density ρ_w. Hence, the wall potential can be written as

$$V(x, z) = \frac{4}{45} \pi \varepsilon_w \rho_w \sigma^3 \left(\frac{\sigma}{z} \right)^9 + V_L(x, z)\,,$$

where the first term is the repulsive part of the Lennard-Jones 9-3 potential, while the second part is the attractive contribution due to the stripe of width L, which can be expressed as

$$V_L(x, z) = -4\varepsilon_w \sigma^6 \rho_w \int_{x-L}^{x} dx' \int_{-\infty}^{\infty} dy' \int_z^{\infty} dz'$$
$$\times \frac{1}{(x'^2 + y'^2 + z'^2)^3} \qquad (37)$$
$$= \alpha_w \left[\frac{1}{(x - L)^3} - \frac{1}{x^3} + \psi_6(x - L, z) - \psi_6(x, z) \right]$$
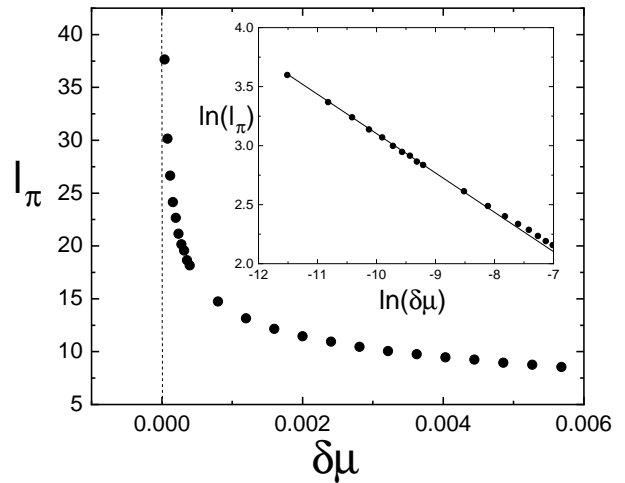
FIG. 2: A dependence of the thickness ℓ_π of the liquid film adsorbed on a planar wall on $\delta\mu = \mu_{\text{sat}} - \mu$ at temperature $T = 0.92\,T_c$. The inset shows the behaviour of $\ell_\pi(\delta\mu)$ near the saturation as a log-log plot; here, the solid line is a linear fit to the data with a slope of $-1/3$ which verifies the expected power-law dependence (9).

where

$$\alpha_w = -\frac{1}{3} \pi \varepsilon_w \sigma^6 \rho_w \qquad (38)$$

and

$$\psi_6(x, z) = -\frac{2\,x^4 + x^2 z^2 + 2\,z^4}{2z^3 x^3 \sqrt{x^2 + z^2}}\,. \qquad (39)$$

The minimization of Eq. (27) leads to the Euler-Lagrange equation for the density profile $\rho(\mathbf{r})$:

$$k_B T \ln[\rho(\mathbf{r})\Lambda^3] + \frac{\delta(\mathcal{F}_{\text{hs}} + \mathcal{F}_{\text{att}})}{\delta\rho(\mathbf{r})} + \mu - V(\mathbf{r}) = 0\,, \quad (40)$$

which is solved iteratively on a two-dimensional grid (x, z) in Cartesian coordinates using the Gaussian quadrature [53].

IV. RESULTS

In this section the predictions obtained in section II are compared with the numerical DFT results. All the results correspond to $\rho_w \varepsilon_w = 1 \cdot \varepsilon \sigma^{-3}$ and temperature $T = 0.92\,T_c = 1.15\,T_w$, where T_c is the bulk critical temperature and T_w is the wetting temperature of the stripe. Since now on, all the length and energy quantities will be expressed in units of σ and ε, respectively.

Prior to discussing adsorption on a stripe of finite width L, let us first consider complete wetting on a homogeneous wall exerting Lennard-Jones 9-3 potential, which corresponds to the limiting case $L \to \infty$ of our substrate model. Fig. 2 displays a dependence of the film thickness

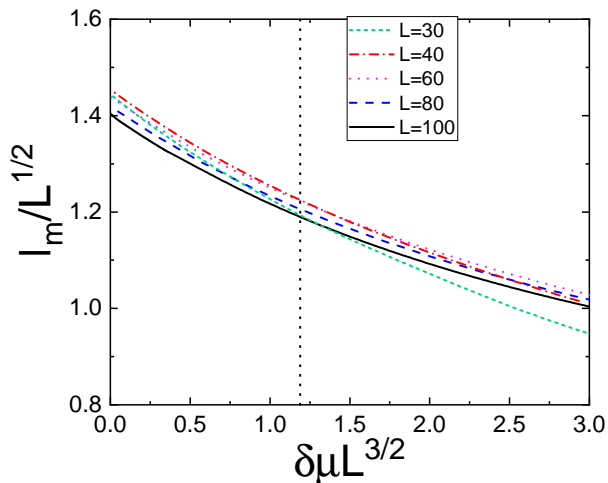FIG. 3: DFT results showing a data collapse for the dependence of ℓ_m on $\delta\mu$ for various values of stripe widths L in rescaled units. The dotted vertical line denotes an estimated borderline beyond which the scaling is not expected to be obeyed anymore.
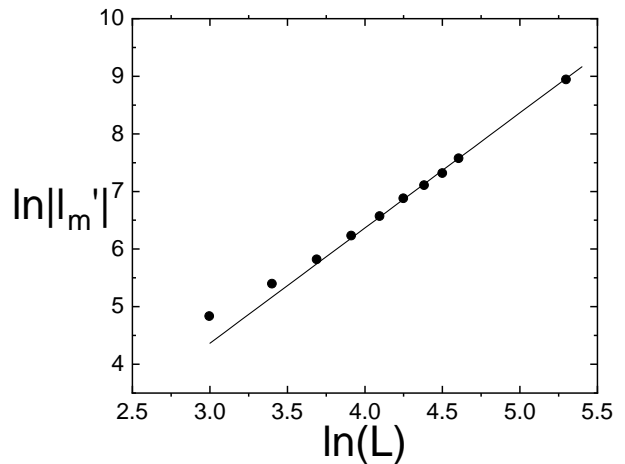

FIG. 4: A log-log plot of the slope of $\ell_m(\delta\mu)$ at $\delta\mu = 0$ for various stripe widths L as obtained from DFT. For $L \geq 40$ the data follow the line with the slope of 2 confirming that $\ell'_m(0) \propto L^2$ as follows from Eq. (20).

ℓ_π on the chemical potential departure from saturation, $\delta\mu$, as obtained from the DFT model formulated in section III. For a given value of $\delta\mu$, the equilibrium density profile $\rho(z)$ is obtained by solving Eq. (40) with the external field $V(z) = 4\pi\varepsilon_w\rho_w\sigma^3\left[1/45\,(\sigma/z)^9 - 1/6\,(\sigma/z)^3\right]$, where z is the distance from the wall. The film thickness ℓ_π is determined from the density profile using the mid-density rule, $\rho(\ell_\pi) = (\rho_g + \rho_l)/2$. In order to accelerate the iteration process near the saturation where ℓ_π grows rapidly, several liquid slabs of different widths were considered first and the one corresponding to the minimal value of the approximate value of the grand potential obtained from (27) after just a few tens of iterations is eventually used as the initial configuration for the full iteration process. In the inset of Fig. 2, the graph is displayed as a log-log plot, which shows a linear dependence with a slope of $-1/3$ for small $\delta\mu$, in accordance with the expected power-law dependence of Eq. (9). Applying the linear regression to the log-log plot, the magnitude of the power-law has been estimated to be roughly 1.3 which allows to determine ℓ_π for further purposes; this value is consistent with that obtained directly from Eq. (9) by substituting for $A = \pi/3\,\rho_w\varepsilon_w\sigma^6\Delta\rho$ [6].

We now turn to complete wetting of a stripe of width L. First of all, we test the asymptotic results for the drop growth in the limit of $\delta\mu \to 0$ as given by Eq. (20). According to this result, there exists a linear regime of $\ell(\delta\mu)$ sufficiently close to the saturation which implies a universal behaviour of the drop growth in the rescaled variables $\widetilde{\delta\mu} = \delta\mu L^{3/2}$ and $\widetilde{\ell_m} = \ell_m/\sqrt{L}$. In Fig. 3, the dependence of $\widetilde{\ell_m}(\widetilde{\delta\mu})$ is displayed for a number of different stripe widths L obtained from DFT. As can be seen, the data indeed almost collapse to a single curve confirming the scaling behaviour for all the considered

stripe widths up to the dotted line which corresponds to the value, for which $\ell_0 \approx \ell_\pi$. Interestingly, the data collapse extends even beyond this threshold except for the most microscopic case of $L = 30$; this reflects the fact that the higher order coefficients in the series expansion decay rather rapidly.

A further test of the scaling properties of the drop growth near the saturation is shown in Fig. 4. Here, a modulus of the derivative of ℓ_m with respect to $\delta\mu$ at $\delta\mu = 0$ is displayed for various values of L. In the log-log plot, the dependence shows a near linear behaviour and follows perfectly the line with a slope of 2 for all the values of $L \geq 40$, which provides a further support of the conclusions drawn from Eq. (20).

Finally, let us compare the truncated series expansions and the rational function approximation with DFT over a large interval of $\delta\mu$, i.e. even well below the saturation. In Fig. 5, the comparison is made between results obtained from the series expansions up to the third order as given by the solution of Eq. (22), the rational function approximation as given by Eq. (26) and DFT for different values of the stripe width. In all the cases, the saturation drop height ℓ_0 as given by DFT has been used as the input to the theories, while the power-law asymptotic form (9) has been used to determine ℓ_π. Since the scaling properties of Eq. (20) has been verified previously, it is not surprising already that the linear approximation captures properly the behaviour of $\ell_m(\delta\mu)$ near the saturation as we can now see explicitly for all the cases. Moreover, we can also see that the linear regime thins with increasing of L, which is in accordance with condition (21). The quadratic and cubic approximations somewhat extend the interval of $\delta\mu$ over which the truncated series expansion provides a reasonable agreement with DFT before they eventually blow up and in fact for the smallest L the accuracy of the cubic approximation is very reason-
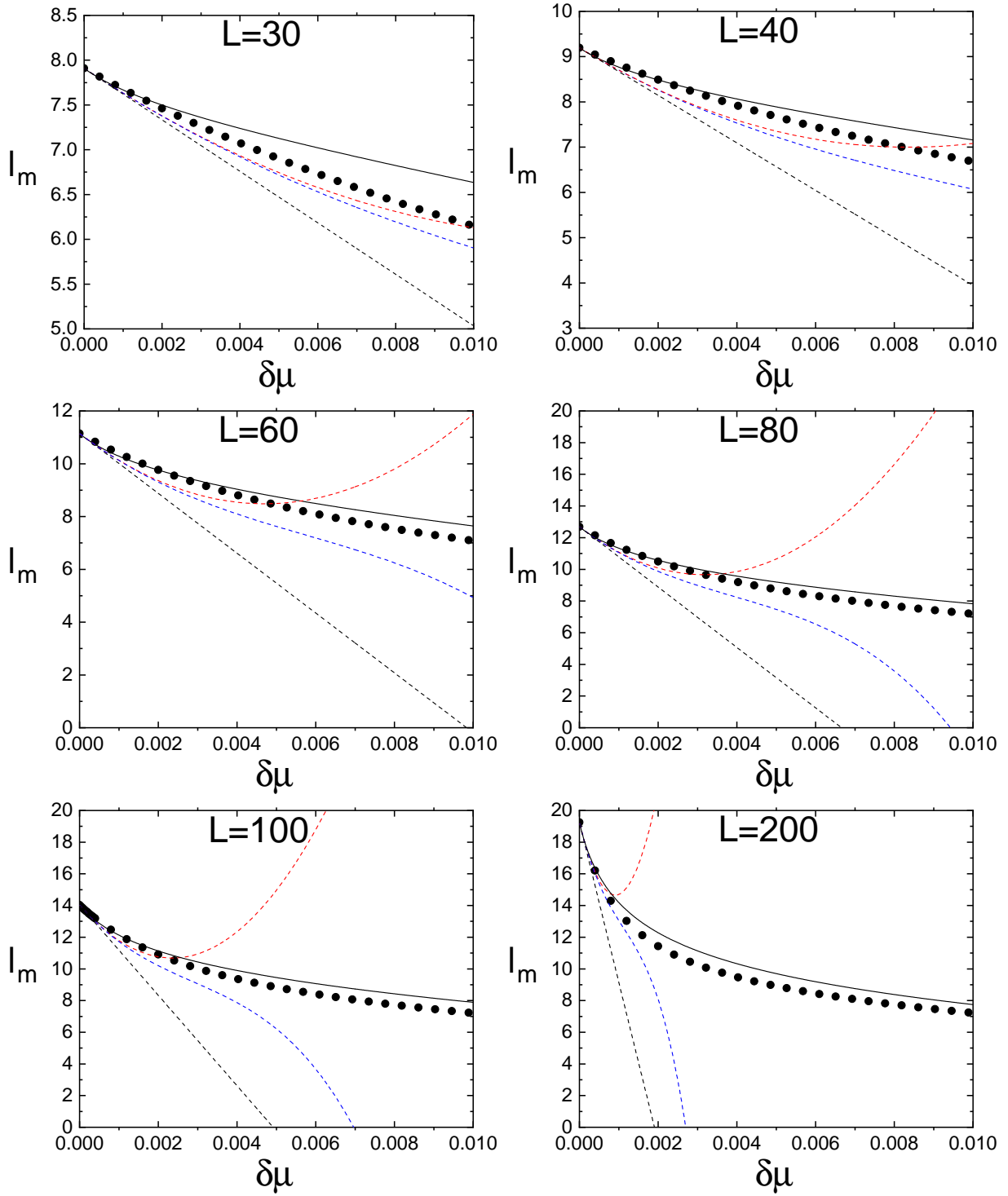
FIG. 5: A comparison between the DFT results (symbols) and the approximative theoretical predictions for various values of the stripe width L. The dashed lines denote linear (black dashed), quadratic (red dashed) and cubic (blue dashed) orders of the expansion series (14) as obtained from the interfacial Hamiltonian model. The black solid line represents the rational function approximation (26).

able over almost the entire range of the considered values of $\delta\mu$. However, the interval of applicability of the higher order expansions also gets more and more narrow as L increases, since the same competition between the stripe width and the parallel correlation function (decreasing with $\delta\mu$) applies. In contrast to the series expansions whose performance worsen by increasing both $\delta\mu$ and L, the simple rational function (26) provides a very reasonable approximation over the whole range of $\delta\mu$ for all the stripe widths; in general, the rational function approximation slightly overestimates the DFT results but the discrepancy never exceeds one molecular diameter.

V. SUMMARY

In this work, complete wetting of a macroscopically long stripe of width L has been studied using mesoscopic and microscopic (DFT) methods. To this end, a wall patterned by a macroscopically long stripe interacting with the fluid via a long-range potential has been considered and the process of increasing the chemical potential (or pressure) towards the saturation was studied. Since the temperature of the system was fixed to the value exceeding the wetting temperature of the stripe and the rest of the wall was considered to be non-wet (purely repulsive in DFT calculations), a liquid drop is adsorbed at the stripe and its height ℓ_m grows continuously as the chemical potential is increased. The purpose of this study was to describe the proces of the droplet growth $\ell(\delta\mu)$ as the saturation $\delta\mu = 0$ is approached where the drop adopts its maximal height $\ell_0 \equiv \ell_m(0)$.

We first presented a mean-field analysis based on an interfacial Hamiltonian model; although the corresponding Euler-Lagrange equation does not provide an exact solution in a closed form for $\delta\mu > 0$, it allows for the low $\delta\mu$ expansion around the saturation for which the exact solution is known. From this it follows that ℓ_0 is approached linearly in $\delta\mu$ with a slope scaling with L^2. These results suggest that there exists a single universal curve of $\ell(\delta\mu)$ to which all adsorption isotherms collapse near the saturation when properly rescaled, such that $\delta\mu \rightarrow \delta\mu L^{3/2}$ and $\ell_m \rightarrow \ell_m/\sqrt{L}$. This regime is restricted by a condition that the parallel correlation function $\xi_\parallel$ pertinent to the stripe is larger than the stripe width L. All these predictions have been confirmed using a microscopic DFT.

According to this analysis, the linear, as well as any higher order regime obtained by truncating the series expansion shrinks with L, which is verified by comparing the results with DFT for a broad range of stripe widths. The comparison has been made for the series expansions up to the third order and although the higher order corrections improve the behaviour of $\ell_m(\delta\mu)$, such that the cubic approximation provides a fairly good agreement with DFT results even well below saturation for stripe widths of few tens of molecular diameters, the series expansion clearly does not represent the most appropriate form of $\ell_m(\delta\mu)$ for large L. Therefore, an alternative approach based on finite-size scaling arguments has been applied requiring the correct behaviour of $\ell_m(\delta\mu)$ for macroscopically wide stripes, such that $\ell_m(L, \delta\mu) \rightarrow \ell_\pi \sim \delta\mu^{-1/3}$ for $L \rightarrow \infty$. Together with a condition that $\ell_m(0) = \ell_0$ this suggests an expression of ℓ_m in a form of a rational function of a single parameter $t = \ell_0/\ell_\pi$, which includes both $\delta\mu$ and L. These conditions require that the degrees of the numerator and denominator polynomials forming the rational function are the same but apart from that there is no other restriction. However, by imposing additionally that the low $\delta\mu$ behaviour of ℓ_m is consistent with the linear regime as determined by the interface Hamiltonian model, it follows that the minimal degree of the rational function is three. Taking into account these conditions, a Padé approximant with a minimal number of terms that are necessary to reproduce the large L and the small $\delta\mu$ behaviour of ℓ_m is constructed. This approximation has been shown to be in a very reasonable agreement with the DFT results for the whole interval of the considered stripe widths ranging from 30 to 200 molecular diameters and even far from the saturation.

Finally, let us note that the mean-field character of the analysis should not debase any of the conclusions made in view of the irrelevant effect of the interfacial fluctuations in the considered three-dimensional substrate model [8], which thus should not disrupt the compactness of the cylindrical droplets. Likewise, the pinning of the droplets at the edges of the stripe is expected to make them resistant towards the Plateau–Rayleigh instability [54, 55]. Among many other potential extensions of this work, let us mention the possibility of the prewetting jump in ℓ_m expected at lower temperatures and the anticipated finite-size shift in the prewetting line. The analysis could also be extended over the saturation, i.e. for $\delta\mu$ negative, which would be relevant e.g. for slits formed of patterned walls with Young's contact angle larger than $\pi/2$. The influence of the substrate geometry on the droplet growth on a wetting patch should also be elucidated. Most notably, experimental verification of our results is desirable. Admittedly, this task is challenging and technically non-trivial. This is not only due to firm requirements of very accurate determination of the undersaturation but mainly because of the need to measure precisely the profile of drops of molecular dimensions. This is in some contrast to macroscopically large drops (whose dimension is comparable with the capillary length) in which case a crossover to the gravity dominated regime causing a drop flattening is already expected. However, the rapidly increasing development of the nanotechnological methods promises a possibility of the experimental test of these predictions in a near future.

[1] J. W. Cahn J. Chem. Phys. **66**, 3667 (1977).
[2] C. Ebner and W. F. Saam, Phys. Rev. Lett. **88**, 1486 (1977).
[3] H. Nakanishi and M. E. Fisher, Phys. Rev. Lett. **49**, 1565 (1982).
[4] D. E. Sullivan and M. M. Telo da Gama, in *Fluid Interfacial Phenomena*, edited by C. A. Croxton (Wiley, New York, 1985).
[5] S. Dietrich, in *Phase Transitions and Critical Phenomena*, edited by C. Domb and J. L. Lebowitz (Academic, New York, 1988), Vol. 12.
[6] M. Schick, in *Liquids and Interfaces*, edited by J. Chorvolin, J. F. Joanny, and J. Zinn-Justin (Elsevier, New York, 1990).
[7] D. Bonn, J. Eggers, J. Indekeu, J. Meunier, and E. Rolley, Rev. Mod. Phys. **81**, 739 (2009).
[8] R. Lipowsky, Phys. Rev. Lett. **52**, 1429 (1984).
[9] E. H. Hauge, Phys. Rev. A **46**, 4994 (1992).
[10] K. Rejmer, S. Dietrich, and M. Napirkówski, Phys. Rev. E **60**, 4027 (1999).
[11] A. O. Parry, C. Rascón, and A. J. Wood, Phys. Rev. Lett. **83**, 5535 (1999).
[12] K. Rejmer, Phys. Rev. E **65**, 061606 (2002).
[13] C. Rascón and A. O. Parry, Phys. Rev. Lett. **94**, 096103 (2005).
[14] L. Bruschi and G. Mistura, J. Low Temp. Phys.**157**, 206 (2009).
[15] F. Ancilotto, M. Barranco, E.S. Hernandez, M. Pi, J. Low Temp. Phys.**157**, 174 (2009).
[16] P. A. Monon, Microp. Mesopor. Mat. **160**, 47 (2012).
[17] C. Rascón, A. O. Parry, R. Nürnberg, A. Pozzato, M. Tormen, L Bruschi, and G. Mistura, J. Phys.: Condens. Matter **25**, 192101 (2013).
[18] A. Malijevský and A. O. Parry, Phys. Rev. Lett. **110**, 166101 (2013).
[19] A. Malijevský and A. O. Parry, J. Phys.: Condens. Matter **25**, 305005 (2013).
[20] A. Malijevský and A. O. Parry, J. Phys.: Condens. Matter **26**, 355003 (2014).
[21] A. O. Parry, A. Malijevský, and C. Rascón, Phys. Rev. Lett. **113**, 146101 (2014).
[22] A. Rodriguez-Rivas, J. Galván, and J. M. Romero-Enrique, J. Phys. Condens. Matter **27**, 035101 (2015).
[23] C. Rascón, A. O. Parry, and A. Santori, Phys. Rev. E **59**, 5697 (1999).
[24] C. Bauer and S. Dietrich, Phys. Rev. E **61**, 1664 (2000).
[25] C. Rascón and A. O. Parry, J. Phys.: Condens. Matter **12**, A369 (2001).
[26] G. P. Fang and A. Amirfazli, Langmuir **28**, 9421 (2012).
[27] A. Malijevský, Phys. Rev. E **99**, 040801 (2019).
[28] A. Malijevský, Phys. Rev. E **102**, 012804 (2020).
[29] M. Schoen, Phys. Chem. Chem. Phys. **10**, 223 (2008).
[30] S. P. Li, Y. T. Chun, S. Zhao, H Ahn, D. Ahn, J. I. Sohn, Y. B. Xu, P. Shrestha, M Pivnenko, D. P. Chu, Nat. Comun. **9**, 393 (2018).
[31] A. Malijevský, A. O. Parry, and M. Pospíšil, Phys. Rev. E **99**, 042804 (2019).
[32] P. Lenz and R. Lipowsky, Phys. Rev. Lett. **80**, 1920 (1998).
[33] C. Bauer, S. Dietrich, and A. O. Parry, Europhys Lett. **47**, 474 (1999).
[34] H. Gau, S. Herminghaus, P. Lenz, and R. Lipowsky, Science **283**, 486 (1999).
[35] K. Kargupta and A. Sharma, J. Chm. Phys. **116**, 3042 (2002).
[36] M. Geoghegan and G. Krausch, Prog. Polym. Sci. bf 28, 261 (2003).
[37] J. Z. Wang, Z. H. Zheng, H. W. Li, W. T. S. Huck, and H. Sirringhaus, Nat. Mater. **3**, 171 (2004).
[38] R. Seemann, M. Brinkmann, E. J. Kramer, F. F. Lange, and R. Lipowsky, Proc. Natl. Acad. Sci. U.S.A. **102**, 1848 (2005).
[39] S. Herminghaus, M. Brinkmann, and R. Seemann, Annu. Rev. Mater. Res. **38**, 101 (2008).
[40] S. Dietrich, M. Rauscher, and M. Napiorkowski, in *Nanoscale Liquid Interfaces*, edited by Ondarçuhu T. and Aimé J.-P. (Pan Stanford, Singapore) 2013, p. 83.
[41] M. Dokowicz and W. Nowicki, Int. J. Heat Mass Transf. **115**, 131 (2017).
[42] M. Pospíšil, M. Láska, and A. Malijevský, Phys. Rev. E **100**, 062802 (2019).
[43] A. O. Parry, E.D. Macdonald, and C. Rascón, J. Phys.: Condens. Matter **13**, 383 (2001).
[44] P. Jakubczyk and M. Napiorkowski, J Phys. Condens. Matter **16**, 6917 (2004).
[45] P. Jakubczyk, A. O. Parry, and M. Napiorkowski, Phys. Rev. E **74**, 031608 (2006).
[46] P. Jakubczyk and M. Napiorkowski, J Phys. A-Math. Theor. **40**, 2263 (2007).
[47] M. L. Trobo, E. V. Albano, and K. Binder, Phys. Rev. E **93**, 052805 (2016).
[48] A. Malijevský, A. O. Parry, and M. Pospíšil, , Phys. Rev. E **96**, 032801 (2017).
[49] R. Evans, Adv. Phys. **28**, 143 (1979).
[50] R. Evans in *Fundamentals of Inhomogeneous Fluids*, (New York: Dekker 1992).
[51] J. A. Barker and D. Henderson, J. Chem. Phys. **47**, 4714 (1967).
[52] Y. Rosenfeld, Phys. Rev. Lett. **63**, 980 (1989).
[53] A. Malijevský, J. Phys.: Cond. Matter **25**, 445006 (2013).
[54] J. A. F. Plateau, *Statique Exprimentale et Thorique des Liquides Soumis Aux Seules Forces Molculaires, vol. 2,* Gauthier-Villars, (1873).
[55] L. Rayleigh, Proc. Lond. Math. Soc. **s1-10**, 4 (1878).